

Spin-Orbit Interaction in GaN/Al_xGa_{1-x}N Heterojunctions Probed by Electron Spin Resonance

A.V. Shchepetilnikov^{1,2,*}, A.R. Khisameeva,¹ V.V. Solovyev¹, A. Großer,³ T. Mikolajick,^{3,4} S. Schmult,⁴ and I.V. Kukushkin¹

¹ Institute of Solid State Physics RAS, 142432 Chernogolovka, Moscow District, Russia

² National Research University Higher School of Economics, 101000 Moscow, Russia

³ NaMLab gGmbH, Nöthnitzer Straße 64 a, 01187 Dresden, Germany

⁴ Electrical and Computer Engineering, Institute of Semiconductors and Microsystems, TU Dresden, Nöthnitzer Straße 64, 01187 Dresden, Germany

(Received 2 February 2022; revised 13 June 2022; accepted 11 July 2022; published 12 August 2022)

Fundamental aspects of spin-orbit interaction in commercially relevant GaN/Al_xGa_{1-x}N heterostructures hosting two-dimensional electron systems are extensively studied by electron spin resonance (ESR). This unprecedentedly accurate experimental technique allows access to the fine details of coupling between the spin degree of freedom and the quantized orbital motion of an electron in the quantum Hall regime through the precise measurement of the electron *g*-factor. Filling-factor-dependent changes of the *g*-factor value in strong magnetic fields allow extraction of the Rashba spin-orbit interaction constant α in various GaN/Al_xGa_{1-x}N heterojunctions with electron sheet densities in the range $0.8\text{--}5.2 \times 10^{12} \text{ cm}^{-2}$. Despite three significantly different approaches used to tune the electron density, the extracted value of α is on the order of $5.3 \pm 0.4 \text{ meV Å}$ for all experimental realizations. This striking finding can be explained by assuming that the spin-orbit interaction is of bulk origin. Theoretical calculations confirm this observation, as the bulk cubic in-plane wave-vector term of the spin-orbit interaction compensates the rising contribution due to the change in the quantum well shape. Finally, the value of α is cross-checked and confirmed by weak antilocalization measurements in the longitudinal magnetoresistance at substantially lower magnetic field values compared to the ESR approach. The presented experimental findings provide knowledge for estimating the true scales of spin-orbit interaction in GaN-based spintronic devices.

DOI: 10.1103/PhysRevApplied.18.024037

I. INTRODUCTION

The most prominent properties of GaN include its large direct band gap, outstanding semiconducting properties, chemical stability, and mature epitaxial growth technologies. Therefore, GaN-based low-dimensional systems are often viewed as a promising material platform with plentiful possible applications in the fields of optoelectronics [1–3], high power [4], high frequency [5] and transparent electronics [6], and even spintronics [7–12]. The key to realizing the full potential of this material in the spin electronics is understanding the spin-orbit interaction (SOI), as SOI not only governs the spin relaxation rates, but may be utilized to manipulate the electron spin degree of freedom, as well. Note that the wurtzite structure of GaN implies the absence of an inversion center and thus this material exhibits strong SOI even in the bulk material. Presence of the high-symmetry hexagonal *c*-axis in GaN dictates [13]

the SOI term in the single-electron Hamiltonian to be of the Rashba form [14]:

$$H = \alpha(\boldsymbol{\sigma} \times \mathbf{k}) \cdot \mathbf{n}. \quad (1)$$

Here $\boldsymbol{\sigma}$ stands for the Pauli matrices, whereas \mathbf{k} and \mathbf{n} stand for the electron wave vector and the unity vector directed along the *c* axis, respectively. The value α is an even function of the wave vector k and is constant to the first order in k . This bulk spin-orbit coupling is therefore inherited to GaN-based semiconductor heterostructures.

The constant α and its functional dependence on the electron wave vector in GaN-based devices has been extensively investigated theoretically [15–18], yet the experimental research was limited to solely magneto-transport studies of either thin doped GaN layers or GaN/Al_xGa_{1-x}N heterostructures, namely, to the analysis of the antilocalization traces [19–23] at low magnetic fields or beating patterns [24] of Shubnikov-de Haas oscillations. Note that weak-antilocalization experiments yield SOI constants that are sensitive to the theory used [22],

*shchepetilnikov@issp.ac.ru

whereas the beating patterns approach can be strongly obscured by the possible inhomogeneity of the electron density in the two-dimensional (2D) channel.

Our present work aims to considerably extend the experimental scope of the problem by applying an alternative method of probing spin-orbit parameters with the help of electron spin resonance (ESR) in wurtzite GaN/Al_xGa_{1-x}N heterojunctions hosting a high-quality two-dimensional electron system (2DES) with sheet densities varied in a rather broad range.

The possibility to study spin-orbit interaction by ESR has already been discussed earlier—either by analyzing the *g*-factor anisotropy for the case of GaAs-based heterostructures [25–27], or by studying the modification of the *g* factor in the quantum Hall regime for the case of cubic AlAs quantum wells [28,29]. However, here we use the ESR technique to study SOI in wurtzite GaN-based heterojunctions, which are extremely relevant in the field of applied physics. It is worthwhile to note, that a different crystal symmetry will result in another dominating SOI for the case of GaN-based heterostructures than found in heterostructures containing AlAs or GaAs quantum wells.

The experimental approach utilized is discussed in details in our previous publications [28,29], where it was used to investigate SOI in AlAs-based 2DES. Here we would like to present only a brief summary. At high magnetic fields the in-plane motion of the electrons is quantized in the set of spin-split Landau levels. Yet, spin-orbit interaction is not diagonal in this wave-function basis and hybridizes the states with different Landau level indices and spin projections, leading to the modification of both, the single-particle spin splitting and the correspondent *g* factor. This effect may be easily understood if we analyze the single-electron Hamiltonian in the presence of a strong magnetic field. In the symmetric gauge the wave-vector operators may be expressed as a linear combination of creation and annihilation operators a^+ , a . In this case, the Rashba SO term consists of the products of two operators a or a^+ and σ_+ or σ_- , where $\sigma_{\pm} = (\sigma_x \pm i\sigma_y)/2$ are the spin rotation operators. Each product has a simple physical meaning—the transfer of an electron between neighboring Landau levels with a flip of its spin. In the limit of large magnetic fields, i.e., when the cyclotron splitting is much larger than the characteristic energy of SO interaction α/l_b^2 (l_b stands for the magnetic length), the SO term may be treated as a small perturbation. Using the second-order perturbation theory we may deduce the SOI-induced variation of the *g* factor in the following form [30]:

$$\delta g^* = -A\alpha^2(2N + 1)/B. \quad (2)$$

Here N stands for the Landau-level index, B is the magnetic field and A is a constant consisting of the GaN band parameters. This modification may be probed by

ESR with exceptional accuracy allowing for the precise determination of α .

II. METHODS AND SAMPLES

The spin resonance of the 2D conduction electrons may be detected by monitoring the magnetoresistance R_{xx} of the two-dimensional system in the quantum Hall regime under microwave irradiation. As R_{xx} is extremely sensitive to the microwave absorption, ESR may be observed as a sharp peak in the 2D channel resistance if the magnetic field is swept while the microwave frequency is kept constant. One of the key advantages of this method is that it remains effective in the extremely wide range of fields and microwave frequencies. It was earlier used in Ref. [31] to study ESR in GaAs/(Al, Ga)As heterostructures, and in the case of GaN-based systems the possibility to observe ESR in such a manner was demonstrated recently [32] and was used to measure the spin relaxation rate in these structures. The substantial increase in the signal-to-noise ratio may be achieved by applying the standard double lock-in technique. An alternating probe current of 1 μ A at a frequency of approximately 1 kHz is applied from source to drain. The first lock-in amplifier measures the 2D channel resistance R_{xx} through two sense contacts along the mesa. The sample is irradiated by a sub-THz radiation. As the radiation is 100% amplitude modulated at a frequency of $f_{mod} \sim 30$ Hz, the output signal of the lock-in amplifier contains the oscillating part proportional to the variation of the sample resistance due to the radiation absorption. The second lock-in amplifier, synchronized at f_{mod} , is connected to this output and, thus, measures this variation δR_{xx} .

The sub-THz power is delivered through a cylindrical oversized waveguide. Several backward-wave oscillators serve as sources of microwave radiation covering the frequency range from 65 GHz up to 380 GHz. The microwave radiation power coupled into the waveguide did not exceed 1 mW. The experiments are carried out in the regime of linear response with respect to the power of the microwave radiation and the magnitude of the applied current. We keep the frequency of the sub-THz radiation constant, while the magnetic field is slowly swept allowing us to observe a sharp peak in the variation δR_{xx} of the sample magnetoresistance. As the typical linewidth of the detected peaks is on the order of several mT, the resonant magnetic field of the ESR can be determined with high accuracy. Furthermore, we perform additional testing to check that the effect of nuclear dynamic polarization [33] is negligible and did neither affect the position, nor the line shape of the observed electron spin resonances.

The spin splitting measured with ESR is essentially of single-particle nature, as any many-electron contributions are forbidden by the Larmour theorem. Strictly speaking, in the quantum Hall effect (QHE) regime, ESR implies

resonant absorption of the radiation quanta accompanied by the creation of a spin exciton—the bound state formed from the excited electron in the upper spin-split Landau level and the remnant hole in the lower one. The dispersion calculated in Ref. [34] starts from the purely single-particle Zeeman energy and rises quadratically with the exciton wave vector. As the wave vector of sub-THz light is negligibly small compared to the value $1/l_b$ that sets the wave-vector scale of the spin exciton dispersion, the energy of the absorbed light is exactly the single-particle spin splitting in full accordance with the Larmour theorem.

The experiments are performed on a set of GaN/Al_xGa_{1-x}N heterojunctions grown by molecular beam epitaxy along the *c* direction on Ga-polar, semi-insulating wurtzite GaN bulk substrates. The layer stack consists of a 1-μm-thick GaN buffer followed by a 16-nm-thick (Al, Ga)N barrier and a 3-nm-thick GaN cap. The 2DES is hosted at the GaN/Al_xGa_{1-x}N interface. The growth procedure for these exact structures is reported earlier [35,36]. Typical low-temperature electron sheet density and mobility are equal to $1.7 \times 10^{12} \text{ cm}^{-2}$ and $1.3 \times 10^4 \text{ cm}^2/\text{V s}$, respectively, in case the Al mole fraction is equal to $x = 0.06$. In order to perform magnetotransport measurements a 200-μm-wide Hall bar is patterned from the sample with Ohmic contacts formed by a standard Ti/Al/Ni/Au thermally annealed metal stack. We want to highlight, that several essentially distinct methods of density modification are used, namely, optical pumping with UV light [37], application of external gating, and changing the Al concentration in the barrier region from $x = 0.06$ to $x = 0.25$ [38]. This allows us to study SO interaction in a rather wide range of electron densities and also to check if SOI is sensitive to the way the electron concentration is varied.

Note that in the dark ungated GaN/Al_xGa_{1-x}N heterojunctions under study are insulating in case $x = 0.06$, as 2DES is absent. In case the Hall bar is irradiated with UV light, the 2D channel emerges and persists at low temperatures. After the UV light is turned off, the electron density relaxes to an equilibrium density that is stable on the time scale of several days. This effect is discussed in details elsewhere [37,39]. The stable sheet density is independent of the radiation power, but under constant radiation the value of n is defined by the level of UV light intensity. This enables us to vary the electron density, yet in a rather limited range.

In case the Al mole fraction in the barrier region is increased to $x = 0.25$, the GaN/Al_xGa_{1-x}N heterojunction becomes conductive even in the dark. The corresponding electron concentration reaches the value of $5.2 \times 10^{12} \text{ cm}^{-2}$. Even at such high density only single size quantized subband is populated, as demonstrated by optical studies in Ref. [38]. Extensive magnetotransport and magneto-optical studies of this particular sample may be found in the above cited publication, as well.

The cross section of the sample with $x = 0.06$ and a top gate is demonstrated in the inset of the Fig. 1(a). On the surface of the mesa a 175-nm-thick layer of insulating Al₂O₃ is deposited by atomic layer deposition and is followed by a thin chromium top gate thermally evaporated in a vacuum chamber. We want to highlight that the presence of the external metallic gate noticeably complicates ESR spectroscopy of 2DES, as the electromagnetic radiation is unable to penetrate a highly conducting metallic film. In order to circumvent that obstacle, a top gate with the conductivity below the impedance of free space should be used. In this case a substantial part of the radiation power in the desired frequency range (50–500 GHz) is transmitted through the metallic layer [40]. Thin layers of Cr may serve as ideal candidates for such semitransparent

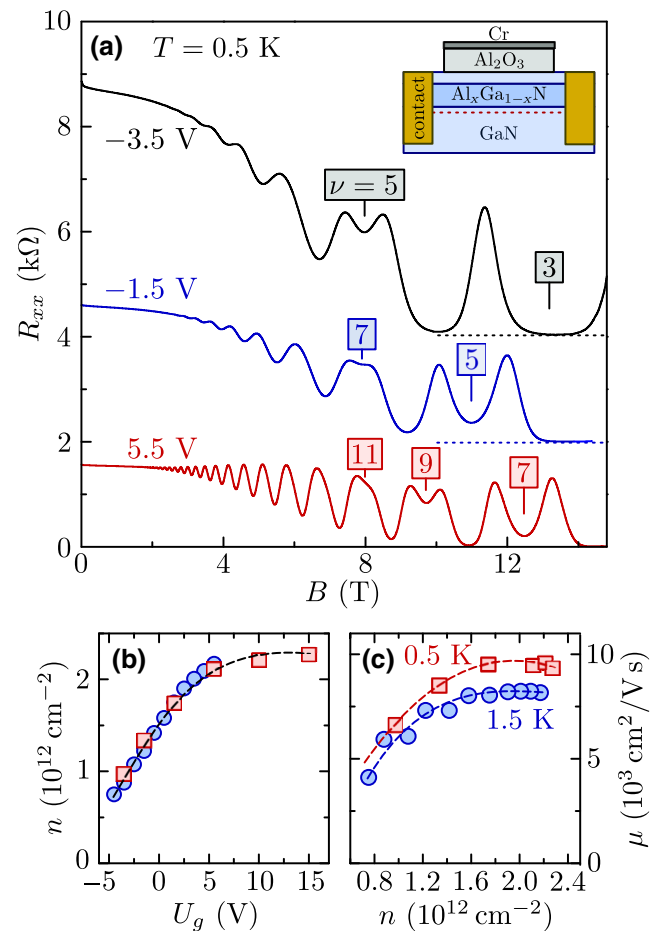


FIG. 1. (a) Typical magnetoresistance of the gated GaN/Al_{0.06}Ga_{0.94}N device in the regime of the QHE for three different top-gate voltages -3.5 , -1.5 , and 5.5 V. The positions of the first several odd filling factors ν are indicated. The temperature is 0.5 K. (b) The dependence of the electron density on the applied top-gate voltage for two temperatures 1.5 K (circles) and 0.5 K (squares). (c) The mobility of the 2D channel versus the 2D electron density for two temperatures 1.5 K (circles) and 0.5 K (squares).

gates due to the good adhesion of Cr and its large sheet resistance at a reasonable layer thickness. The actual thickness of Cr used is in the range of 7 nm. In this case, the typical resistance of the top gate is 1 k Ω per square and is larger than the impedance of free space $Z_0 = 377 \Omega$, allowing the radiation to reach the 2DES. Typical ESR line observed in a gated sample at $T = 0.5$ K is presented in Fig. 2(c) for the radiation frequency of 319.1 GHz. The gate voltage is equal to $U_g = -3.5$ V resulting in the 2D electron density of $0.9 \times 10^{11} \text{ cm}^{-2}$. Solid line denotes a fit performed following the procedure reported in Ref. [32].

The samples are mounted inside the He-3 chamber of a helium-4 cryostat so that experiments are performed at the temperatures down to 0.5 K and in magnetic fields up to 15 T. Typical magnetoresistance traces recorded for a number of top-gate voltages U_g are demonstrated in Fig. 1(a). The position of several odd filling factors is indicated in the figure. The resultant dependencies of the electron sheet densities n on the gate voltage and of the electron mobility on the value of n are displayed in Figs. 1(b) and 1(c), respectively, for the two temperatures of 0.5 and 1.5 K. Note that even in case U_g equaled zero (or the top gate is floating), the 2D channel exists and the device is conducting. We attribute this effect to the pinning of the Fermi energy at the sample surface due to the formation of surface states that are typically created on the boundary between Al₂O₃ and GaN. The potential variation created by these states may effectively scatter electrons in the 2D channel, as a result the observed mobility maximum in the gated structure is smaller than for an ungated one.

III. EXPERIMENTAL RESULTS

First, let us discuss the acquired results for the ungated structures. Typical ESR lineshapes observed in a GaN/Al_{0.06}Ga_{0.94}N structure are demonstrated in Ref. [32]. Given the magnetic field position B_0 of the spin resonance under constant microwave irradiation with frequency F the electron g factor may be calculated as $g = hF/\mu_B B_0$ where h is the Planck constant and μ_B stands for the Bohr magneton. The dependence of the g factor on the magnetic field measured in an ungated structures is presented in the case of $n = 1.7 \times 10^{12} \text{ cm}^{-2}$ in Ref. [32]. UV irradiation enables us to increase the concentration up to $n = 2.2 \times 10^{11} \text{ cm}^{-2}$ and the g factor measured under these conditions is plotted (red symbols and lines) versus the magnetic field B in Fig. 2(a). In the same figure, a similar dependence is demonstrated for the sample with a larger Al fraction $x = 0.25$ (green circles and lines). All these dependencies including that reported in Ref. [32] share the same key features. Increasing magnetic field results in the growth of the g factor. The value of g experiences well-resolved jumps near even filling factors, whereas at the exact odd fillings g is a function of the filling factor ν in full agreement with Eq. (2). The experimental data are

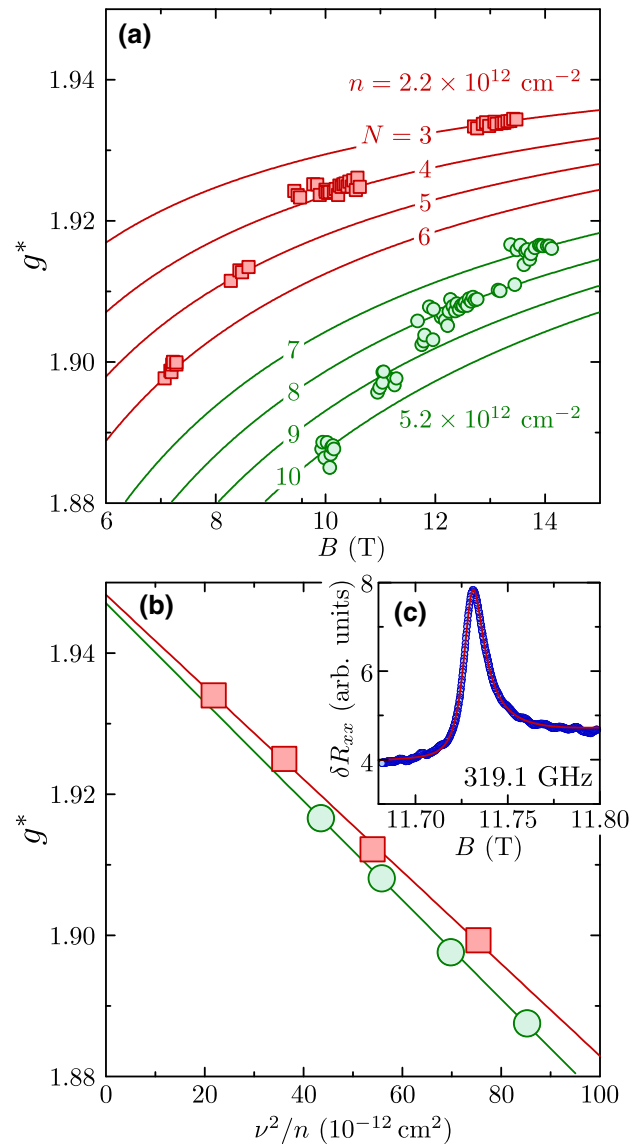


FIG. 2. (a) The dependence of the electron g factor on the magnetic field for several odd fillings $\nu = 2N + 1$. The Landau level indices N are shown near each dataset. The samples studied are two GaN/Al _{x} Ga_{1- x} N structures with the Al mole fractions of $x = 0.06$ (red squares) and $x = 0.25$ (green circles). The corresponding electron density is indicated near each dataset. The solid lines represent the fits according to Eq. (2). The Landau level indices N used correspond to the filling factor $\nu = 2N + 1$. (b) The dependence of the electron g factor on the value of ν^2/n at exact odd fillings for the same two structures as in (a). (c) Typical ESR line observed in a gated sample at $T = 0.5$ K. The radiation frequency is set to 319.1 GHz. The gate voltage is equal to $U_g = -3.5$ V resulting in the 2D electron density of $0.9 \times 10^{11} \text{ cm}^{-2}$. Solid line denotes a fit performed following the procedure reported in Ref. [32].

well fitted by this equation, as can be seen from Fig. 2(a), where fits are denoted with solid lines. The corresponding Landau level indices N used in Eq. (2) are indicated near

each curve and the experimental data obtained near each odd filling $\nu = 2N + 1$ is fitted with a separate line.

Even more convincing is the agreement between the theoretical model and the data if we consider the value of the electron g factor at exactly odd fillings $\nu = 2N + 1$. In this case, Eq. (2) is modified to become

$$g^* - g_0 \sim \alpha^2 \nu^2 / n. \quad (3)$$

Hence, the value of g should be linearly proportional to the combination of ν^2/n with the slope determined solely by the combination of known material parameters and the Rashba coefficient squared. The experimental dependencies of the g factor on the value of ν^2/n are plotted in Fig. 2(b) for the two electron densities $n = 2.2$ and $5.2 \times 10^{12} \text{ cm}^{-2}$ and both of them clearly follow the experimentally expected linear behavior. The linear fits of the data yield very close slopes and, thus, the α coefficients are almost the same. The resultant values of α obtained in ungated samples are demonstrated in Fig. 3(a) for all three electron densities studied. The dependence of α on n is almost absent. We want to highlight that the band nonparabolicity does not affect the value of α determined in such a way, as the value of g at exact odd fillings is proven to be insensitive to this effect [41,42].

The procedure of determining α for gated structures is essentially the same as that for ungated devices. The only experimental difference lays in the slightly reduced quality of the gated structures and, as a result, in the limited amount of odd filling factors that could be examined. The dependencies of the g factor on the parameter ν^2/n for two values of $n = 1.74$ and $2.24 \times 10^{12} \text{ cm}^{-2}$ are presented in Fig. 3(b). Once again both of them are linear and follow each other closely with almost identical slopes and, hence, Rashba coefficients. The resulting dependency of α on electron density demonstrated in Fig. 3(a) turned out to be essentially weak, similar to that of ungated structures. Note that the extracted values of α are slightly larger in gated devices than in those without external gates. This somewhat small discrepancy might stem from the modification of the quantum well shape in the presence of surface states [44] at the $\text{Al}_2\text{O}_3/\text{GaN}$ interface that may induce Fermi-energy surface pinning.

Finally, the Rashba coefficients are also extracted with the aid of a more conventional method, namely, by analyzing the weak antilocalization (WAL) effect in the very same structures. This effect stems from the quantum interference of electron wave functions in the presence of SO interaction [45]. Typical normalized magnetoconductivity with a clear presence of antilocalization is demonstrated in Fig. 3(c) for an ungated $\text{GaN}/\text{Al}_x\text{Ga}_{1-x}\text{N}$ device with $n = 1.7 \times 10^{12} \text{ cm}^{-2}$. Using equations reported in Refs. [19,43] for the case of GaN-based 2DES we may fit the experimental data and deduce the Rashba coefficients. Note that the theoretical model utilized in the cited publications is valid

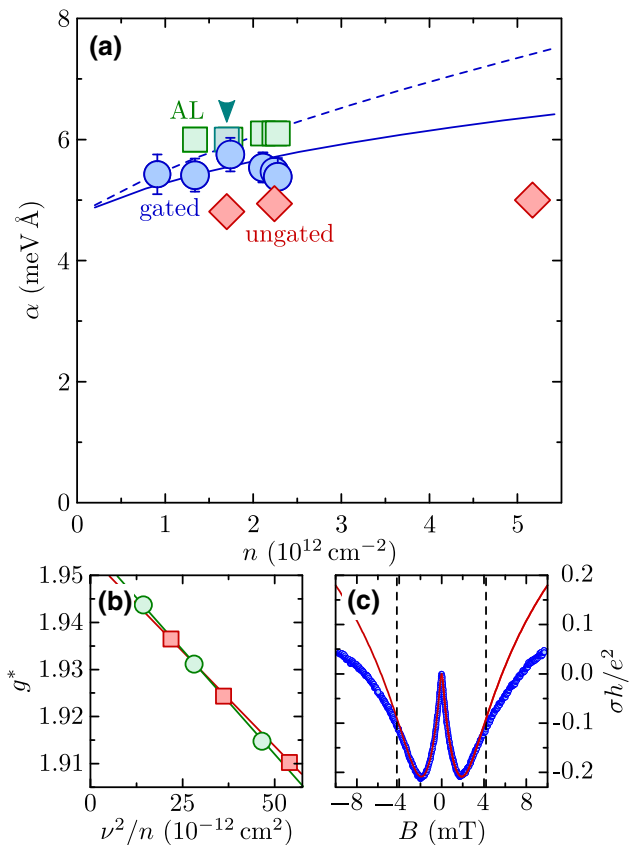


FIG. 3. (a) The value of Rashba coefficient α determined experimentally using various methods. The red diamonds and blue circles denote the α extracted from ESR measurements on the ungated and gated samples, respectively. Green squares denote the Rashba coefficients acquired from fitting the low-field magnetotransport curves with a clear antilocalization effect. The arrow indicates the data point for an ungated $\text{GaN}/\text{Al}_{0.06}\text{Ga}_{0.94}\text{N}$ heterojunction, whereas all the other AL points are measured on the gated device. Solid and dashed lines denote the calculated value of α using Eq. (5) with and without the term $2\pi\gamma n$. (b) The dependence of the electron g factor on the value of ν^2/n at exact odd fillings for the gated $\text{GaN}/\text{Al}_{0.06}\text{Ga}_{0.94}\text{N}$ heterojunction with two different gate voltages of 1.5 and 10 V. The corresponding densities are 1.74 (green circles) and $2.24 \times 10^{12} \text{ cm}^{-2}$ (red squares). (c) The magnetotransport data with a clear AL effect measured on an ungated $\text{GaN}/\text{Al}_{0.06}\text{Ga}_{0.94}\text{N}$ sample. Data are shifted vertically so that $\sigma = 0$ at zero magnetic field. The electron density is equal to $1.7 \times 10^{12} \text{ cm}^{-2}$. Temperature is fixed at 0.5 K. Solid line represents approximation of the data using equations from Ref. [43]. Vertical dashed lines denote the value of transport magnetic field limiting the applicability of the used WAL theory.

in the diffusive regime, i.e., it holds true in the region of magnetic fields smaller than the so-called transport field $B_{\text{tr}} = \hbar/2el^2$, where l is the electron mean free path. The value of B_{tr} is indicated with vertical dashed lines. As can be seen, the experimental data is fitted well with the

theoretical formula in case $B < B_{\text{tr}}$, whereas discrepancy becomes substantial outside this region.

The extracted SO coupling parameters α are summarized in Fig. 3(a). We want to highlight several aspects of the data extracted from WAL. The WAL experiments are carried out in the magnetic field range of several mT in contrast to ESR studies that are performed in the fields several orders of magnitude larger (up to 15 T). Yet the values α determined from WAL compare well with those acquired from ESR experiments and are only a bit larger. Furthermore, they are in excellent qualitative agreement with the AL data reported by other groups [19,21]. The coefficient α extracted from weak antilocalization traces is reported to depend slightly on the theory used [22,46]. This fact may be responsible for the observed deviation. The Rashba coefficients deduced from WAL turned out to be the same for both gated and ungated structures [the data point for an ungated GaN/Al_{0.06}Ga_{0.94}N heterojunction is indicated with an arrow in Fig. 3(a)], suggesting that the accuracy of the used WAL approach is inferior to the ESR experiments. Moreover, we did not observe weak antilocalization for the smallest and highest densities, yet we are able to probe SO interaction by ESR in these structures.

IV. DISCUSSIONS

Both ESR and WAL approaches yield similar results, as not only the extracted values of α are close, but its behavior with varying density is essentially the same. The dependence of the Rashba coefficient on the density is almost absent suggesting the bulk origin of SOI. In order to further understand this result, let us examine closely the structure of α as a function of the electron wave vector. Note that it is recently demonstrated [18] that SO interaction induced by the structural asymmetry of the GaN/Al_xGa_{1-x}N heterostructure is negligibly small, thus later on we focus on the SO coupling inherited from the bulk GaN crystal. The SO interaction to the third order in the wave vector may be written as

$$H_{\text{SO}} = (\alpha_0 + b\gamma k_z^2 - \gamma k_{\parallel}^2)(\sigma_x k_y - \sigma_y k_x). \quad (4)$$

Here α_0 and γ stand for bulk Rashba and Dresselhaus constants, respectively, whereas σ represents Pauli matrices and b is a constant equal to 3.9 in the case of GaN [17]. In quasi-2DES the term k_z^2 becomes a parameter dependent on the well shape, as the movement of electrons in the growth direction is quantized in the size quantized subbands. The value of $\langle k_z^2 \rangle$ is estimated numerically with a self-consistent one-dimensional (1D) Schrödinger-Poisson solver. As the actual form of the quantum well may be affected by several parameters [44], including background doping and surface potential, we had to make several assumptions. Following Ref. [44], the Fermi energy is believed to be pinned in the middle between the

conduction and valence band on the substrate side. Next, the background doping is neglected and the barrier height is supposed to be infinite. Note that under these assumptions the value of $\langle k_z^2 \rangle$ is overestimated, so the actual contribution from the term $b\gamma \langle k_z^2 \rangle$ should be smaller.

The term γk_{\parallel}^2 can be taken into account by using the stationary perturbation theory of the second order on the whole SO Hamiltonian in Eq. (4). It is convenient to rewrite it using operators $\sigma_{\pm} = 1/2(\sigma_x \pm i\sigma_y)$ and $k_{\pm} = k_x \pm ik_y$. Note that in the quantizing magnetic field k_{\pm} are directly related to the creation and annihilation operators a^+ and a representing the transfer of an electron to the next upper or lower Landau level: $k_+ = \sqrt{2}a^+/l_b$ and $k_- = \sqrt{2}a/l_b$. The resulting correction in the limit of $v^2 \gg 1$ and leaving only the linear term in γ can be deduced for the exact odd filling giving the final formula for the α coefficient:

$$\alpha = \alpha_0 + b\gamma \langle k_z^2 \rangle - 2\pi\gamma n. \quad (5)$$

The value of γ is calculated in Ref. [17] to equal 0.32 eV Å³. In order to match the data the α_0 is put to be 4.3 meV Å, which is smaller than the value 9.0 meV Å reported earlier from the theoretical calculations [47]. The values of α calculated according to Eq. (5) is demonstrated by the solid line in Fig. 3(a). The theoretically derived α dependence is rather weak in quantitative agreement with the experimental data. The dashed line in Fig. 3(a) represents the behavior of α if the last term $2\pi\gamma n$ is omitted and here the dependence on the carrier density n is by far stronger compared to the case, when the term is not taken into account. This partly justifies the assumption that the modification of the potential well shape due to the surface charges may alter the value of α . It is worth noting that the surface-induced SO interaction is omitted in the theoretical analysis presented here.

V. CONCLUSIONS

The SO interaction is experimentally probed by the electron spin resonance technique in GaN/Al_xGa_{1-x}N heterojunctions containing high-quality two-dimensional electron systems. ESR is used to measure the single-particle g factor that experiences a SO-induced modification in the quantum Hall regime. The measurements of this phenomenon allowed us to extract the Rashba coefficient in various GaN/Al_xGa_{1-x}N heterojunctions with different electron sheet density. Several distinct methods are used to alter the electron concentration, namely, optical pumping by UV light, electrostatic gate voltage control and changing Al mole fraction in the barrier region. The experimental dependency of the Rashba coefficient on the sheet density is rather weak. This surprising finding suggests the bulk origin of the spin-orbit interaction. Theoretical calculations confirm the statement, as

the cubic in-plane wave-vector term of the Dresselhaus SOI effectively compensates the rising contribution due to the change in the quantum well shape. The Rashba coefficient extracted with the aid of ESR is compared with the values of α determined from WAL measurements. We want to highlight that the ranges of magnetic fields used for WAL and ESR experiments differ by orders of magnitude: several mT for WAL and around 10 T for ESR. Yet a good agreement between the values of α obtained by both of these methods is observed.

ACKNOWLEDGMENTS

The ESR experiments, data analysis, and theoretical modeling are supported by the Russian Science Foundation (Grant No. 20-72-10097). The development of the density variation techniques and transport characterization of the samples are supported by the Russian Foundation for Basic Research (Grant No. 20-02-00426). The NaM-Lab gGmbH part is financially supported by the Deutsche Forschungsgemeinschaft (DFG, German Research Foundation)—Project No. 405782347; the German Federal Ministry of Education and Research—BMBF (Project “ZweiGaN” No. 16ES0145K); and the German Federal Ministry of Economics and Technology—BMWi (Project No. 03ET1398B). The TU Dresden part of the work is partially funded by the DFG Project No. 348524434.

- [1] I. Akasaki and H. Amano, Widegap column-III nitride semiconductors for UV/blue light emitting devices, *J. Electrochem. Soc.* **141**, 2266 (1994).
- [2] K. Akita, T. Nakamura, and H. Hirayama, Advantages of GaN substrates in InAlGaN quaternary ultraviolet-light-emitting diodes, *Jpn. J. Appl. Phys.* **43**, 8030 (2004).
- [3] I. Akasaki, Nobel lecture: Fascinated journeys into blue light, *Rev. Mod. Phys.* **87**, 1119 (2015).
- [4] H. Amano, Y. Baines, E. Beam, M. Borga, T. Bouchet, P. R. Chalker, M. Charles, K. J. Chen, N. Chowdhury, R. Chu, *et al.*, The 2018 GaN power electronics roadmap, *J. Phys. D: Appl. Phys.* **51**, 163001 (2018).
- [5] L. A. Samoska, An overview of solid-state integrated circuit amplifiers in the submillimeter-wave and THz regime, *IEEE Trans. Terahertz Sci. Technol.* **1**, 9 (2011).
- [6] G. Thomas, Invisible circuits, *Nature* **389**, 907 (1997).
- [7] S. Pearton, C. Abernathy, G. Thaler, R. Frazier, D. Norton, F. Ren, Y. Park, J. Zavada, I. A. Buyanova, W. Chen, *et al.*, Wide bandgap GaN-based semiconductors for spintronics, *J. Phys. Condens. Matter* **16**, R209 (2004).
- [8] J. Buß, A. Schaefer, T. Schupp, D. As, D. Hägele, and J. Rudolph, High temperature electron spin dynamics in bulk cubic GaN: Nanosecond spin lifetimes far above room-temperature, *Appl. Phys. Lett.* **105**, 182404 (2014).
- [9] F. Mei, S. Zhang, N. Tang, J. Duan, F. Xu, Y. Chen, W. Ge, and B. Shen, Spin transport study in a Rashba spin-orbit coupling system, *Sci. Rep.* **4**, 1 (2014).
- [10] T.-E. Park, Y. H. Park, J.-M. Lee, S. W. Kim, H. G. Park, B.-C. Min, H.-j. Kim, H. C. Koo, H.-J. Choi, S. H. Han, *et al.*, Large spin accumulation and crystallographic dependence of spin transport in single crystal gallium nitride nanowires, *Nat. Commun.* **8**, 1 (2017).
- [11] E. Vetter, M. Biliroglu, D. Seyitliyev, P. Reddy, R. Kirste, Z. Sitar, R. Collazo, K. Gundogdu, and D. Sun, Observation of carrier concentration dependent spintronic terahertz emission from *n*-GaN/NiFe heterostructures, *Appl. Phys. Lett.* **117**, 093502 (2020).
- [12] X. Liu, N. Tang, S. Zhang, X. Zhang, H. Guan, Y. Zhang, X. Qian, Y. Ji, W. Ge, and B. Shen, Effective manipulation of spin dynamics by polarization electric field in InGaN/GaN quantum wells at room temperature, *Adv. Sci.* **7**, 1903400 (2020).
- [13] M. I. Dyakonov, *Spin Physics in Semiconductors* (Springer-Verlag, Berlin, Heidelberg, 2008).
- [14] Y. A. Bychkov, Properties of 2D electron gas with lifted spectral degeneracy, *JETP Lett.* **39**, 78 (1984).
- [15] L. C. Lew Yan Voon, M. Willatzen, M. Cardona, and N. E. Christensen, Terms linear in k in the band structure of wurtzite-type semiconductors, *Phys. Rev. B* **53**, 10703 (1996).
- [16] W.-T. Wang, C. Wu, S. Tsay, M. Gau, I. Lo, H. Kao, D. Jang, J.-C. Chiang, M.-E. Lee, Y.-C. Chang, *et al.*, Dresselhaus effect in bulk wurtzite materials, *Appl. Phys. Lett.* **91**, 082110 (2007).
- [17] J. Fu and M. Wu, Spin-orbit coupling in bulk ZnO and GaN, *J. Appl. Phys.* **104**, 093712 (2008).
- [18] J. Fu, P. H. Penteado, D. R. Candido, G. J. Ferreira, D. P. Pires, E. Bernardes, and J. C. Egues, Spin-orbit coupling in wurtzite heterostructures, *Phys. Rev. B* **101**, 134416 (2020).
- [19] S. Schmult, M. J. Manfra, A. Punnoose, A. M. Sergent, K. W. Baldwin, and R. J. Molnar, Large Bychkov-Rashba spin-orbit coupling in high-mobility GaN/Al_xGa_{1-x}N heterostructures, *Phys. Rev. B* **74**, 033302 (2006).
- [20] N. Thilloesen, T. Schäpers, N. Kaluza, H. Hardtdegen, and V. A. Guzenko, Weak antilocalization in a polarization-doped Al_xGa_{1-x}N/GaN heterostructure with single subband occupation, *Appl. Phys. Lett.* **88**, 022111 (2006).
- [21] C. Kurdak, N. Biyikli, U. Özgür, H. Morkoç, and V. I. Litvinov, Weak antilocalization and zero-field electron spin splitting in Al_xGa_{1-x}N/AlN/GaN heterostructures with a polarization-induced two-dimensional electron gas, *Phys. Rev. B* **74**, 113308 (2006).
- [22] D. Spirito, L. Di Gaspare, F. Evangelisti, A. Di Gaspare, E. Giovine, and A. Notargiacomo, Weak antilocalization and spin-orbit interaction in a two-dimensional electron gas, *Phys. Rev. B* **85**, 235314 (2012).
- [23] A. E. Belyaev, V. G. Raicheva, A. M. Kurakin, N. Klein, and S. A. Vitusevich, Investigation of spin-orbit interaction in AlGaN/GaN heterostructures with large electron density, *Phys. Rev. B* **77**, 035311 (2008).
- [24] K. Tsubaki, N. Maeda, T. Saitoh, and N. Kobayashi, Spin splitting in modulation-doped AlGaN/GaN two-dimensional electron gas, *Appl. Phys. Lett.* **80**, 3126 (2002).
- [25] Y. A. Nefyodov, A. V. Shchepetilnikov, I. V. Kukushkin, W. Dietsche, and S. Schmult, Electron *g*-factor anisotropy in GaAs/Al_{1-x}Ga_xAs quantum wells of different symmetry, *Phys. Rev. B* **84**, 233302 (2011).

- [26] Z. A. Devizorova, A. Shchepetilnikov, Y. A. Nefyodov, V. Volkov, and I. V. Kukushkin, Interface contributions to the spin-orbit interaction parameters of electrons at the (001) GaAs/AlGaAs interface, *JETP Lett.* **100**, 102 (2014).
- [27] P. Alekseev, Anisotropy of the electron g-factor in quantum wells based on cubic semiconductors, *Semiconductors* **47**, 1241 (2013).
- [28] A. V. Shchepetilnikov, D. D. Frolov, Y. A. Nefyodov, I. V. Kukushkin, L. Tiemann, C. Reichl, W. Dietsche, and W. Wegscheider, Spin-orbit coupling effects in the quantum Hall regime probed by electron spin resonance, *Phys. Rev. B* **98**, 241302 (2018).
- [29] A. V. Shchepetilnikov, A. R. Khisameeva, Yu. A. Nefyodov, I. V. Kukushkin, L. Tiemann, C. Reichl, W. Dietsche, and W. Wegscheider, Spin-orbit interaction in AlAs quantum wells, *Physica E* **124**, 114278 (2020).
- [30] R. Winkler, *Spin-Orbit Coupling Effects in Two-Dimensional Electron and Hole Systems*, Springer Tracts in Modern Physics (Springer, Berlin, 2003), Vol. 191.
- [31] D. Stein, K. v. Klitzing, and G. Weimann, Electron Spin Resonance on GaAs-Al_xGa_{1-x}As Heterostructures, *Phys. Rev. Lett.* **51**, 130 (1983).
- [32] A. V. Shchepetilnikov, D. D. Frolov, V. V. Solovyev, Y. A. Nefyodov, A. Großer, T. Mikolajick, S. Schmult, and I. V. Kukushkin, Electron spin resonance in a 2D system at a GaN/AlGaN heterojunction, *Appl. Phys. Lett.* **113**, 052102 (2018).
- [33] M. Dobers, K. v. Klitzing, J. Schneider, G. Weimann, and K. Ploog, Electrical Detection of Nuclear Magnetic Resonance in GaAs-Al_xGa_{1-x}As Heterostructures, *Phys. Rev. Lett.* **61**, 1650 (1988).
- [34] C. Kallin and B. I. Halperin, Excitations from a filled Landau level in the two-dimensional electron gas, *Phys. Rev. B* **30**, 5655 (1984).
- [35] F. Schubert, S. Wirth, F. Zimmermann, J. Heitmann, T. Mikolajick, and S. Schmult, Growth condition dependence of unintentional oxygen incorporation in epitaxial GaN, *Sci. Technol. Adv. Mater.* **17**, 239 (2016).
- [36] S. Schmult, F. Schubert, S. Wirth, A. Großer, T. Mittmann, and T. Mikolajick, Control of unintentional oxygen incorporation in GaN, *J. Vac. Sci. Technol. B* **35**, 02B104 (2017).
- [37] S. Schmult, S. Wirth, V. V. Solovyev, R. Hentschel, A. Wachowiak, T. Scheinert, A. Großer, I. V. Kukushkin, and T. Mikolajick, Normally-off operation of lateral field-effect transistors fabricated from ultrapure GaN/AlGaN heterostructures, *Phys. Status Solidi (a)* **217**, 1900732 (2020).
- [38] V. V. Solovyev, S. Schmult, L. Krückeberg, A. Großer, T. Mikolajick, and I. V. Kukushkin, Light-tunable 2D subband population in a GaN/AlGaN heterostructure, *Appl. Phys. Lett.* **118**, 013101 (2021).
- [39] L. Krückeberg, S. Wirth, V. V. Solovyev, A. Großer, I. V. Kukushkin, T. Mikolajick, and S. Schmult, Quantum and transport lifetimes in optically induced GaN/AlGaN 2DEGs grown on bulk GaN, *J. Vac. Sci. Technol. B* **38**, 042203 (2020).
- [40] P. A. Gusikhin, V. M. Muravev, K. R. Dzhikirba, A. Shuvayev, A. Pimenov, and I. V. Kukushkin, Effect of a conductive layer on Fabry-Pérot resonances, *Phys. Rev. B* **104**, 115408 (2021).
- [41] M. Dobers, K. v. Klitzing, and G. Weimann, Electron-spin resonance in the two-dimensional electron gas of GaAs-Al_xGa_{1-x}As heterostructures, *Phys. Rev. B* **38**, 5453 (1988).
- [42] Y. A. Nefyodov, A. V. Shchepetilnikov, I. V. Kukushkin, W. Dietsche, and S. Schmult, g-factor anisotropy in a GaAs-Al_xGa_{1-x}As quantum well probed by electron spin resonance, *Phys. Rev. B* **83**, 041307 (2011).
- [43] A. Punnoose, Magnetoconductivity in the presence of Bychkov-Rashba spin-orbit interaction, *Appl. Phys. Lett.* **88**, 252113 (2006).
- [44] T. Scheinert, T. Mikolajick, and S. Schmult, Critical parameters for the presence of a 2DEG in GaN/Al_xGa_{1-x}N heterostructures, *AIP Adv.* **9**, 125018 (2019).
- [45] G. Bergmann, Weak localization in thin films: A time-of-flight experiment with conduction electrons, *Phys. Rep.* **107**, 1 (1984).
- [46] L. E. Golub, Weak antilocalization in high-mobility two-dimensional systems, *Phys. Rev. B* **71**, 235310 (2005).
- [47] J. Majewski and P. Vogl, in *Physics of Semiconductors: 27th International Conference on the Physics of Semiconductors* (American Institute of Physics, New York, 2005), p. 1403.